Twist-to-untwist Evolution and Cation Polarization Behavior of Hybrid Halide Perovskite Nanoplatelets Revealed by Cryogenic Transmission Electron Microscopy

Yuanmin Zhu,[1,2] Shixun Wang,[3] Bai Li,[1] Xuming Yang,[1] Duojie Wu,[1] Shihui Feng,[1] Lei Li,[1*] Andrey L. Rogach,[3] Meng Gu [1*]

[1] *Department of Materials Science and Engineering, Southern University of Science and Technology, Shenzhen 518055, P. R. China*

[2] *Department of Materials Science and Engineering, Dongguan University of Technology, Dongguan 523808, China*

[3] *Department of Materials Science and Engineering, and Centre for Functional Photonics (CFP), City University of Hong Kong, Hong Kong S.A.R., P. R. China*

Contents

1 Schematics

Scheme S1. Illustration of loading the samples in a Cryo-TEM

2 Supplementary Figures
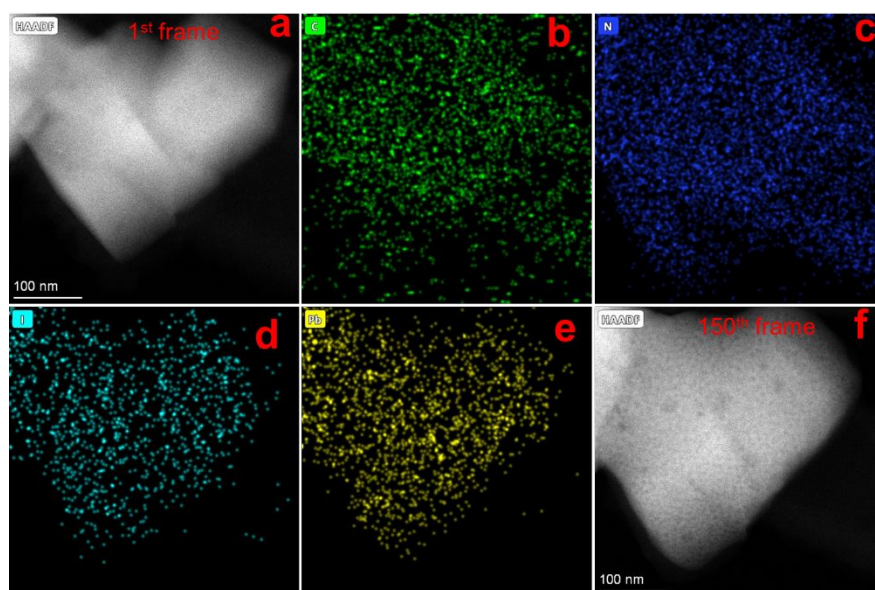### 2.1 STEM-EDS data of nanoplatelets (NPLs)

Fig. S1. EDS data of MAPbI$_3$ NPLs. (a) HAADF image at the first frame and (b-e) the C, N, I, Pb maps. (f) HAADF image at 150 frame (195s) showing obvious beam damage.

2.2 Estimation of thickness of the MAPbI₃ NPLs
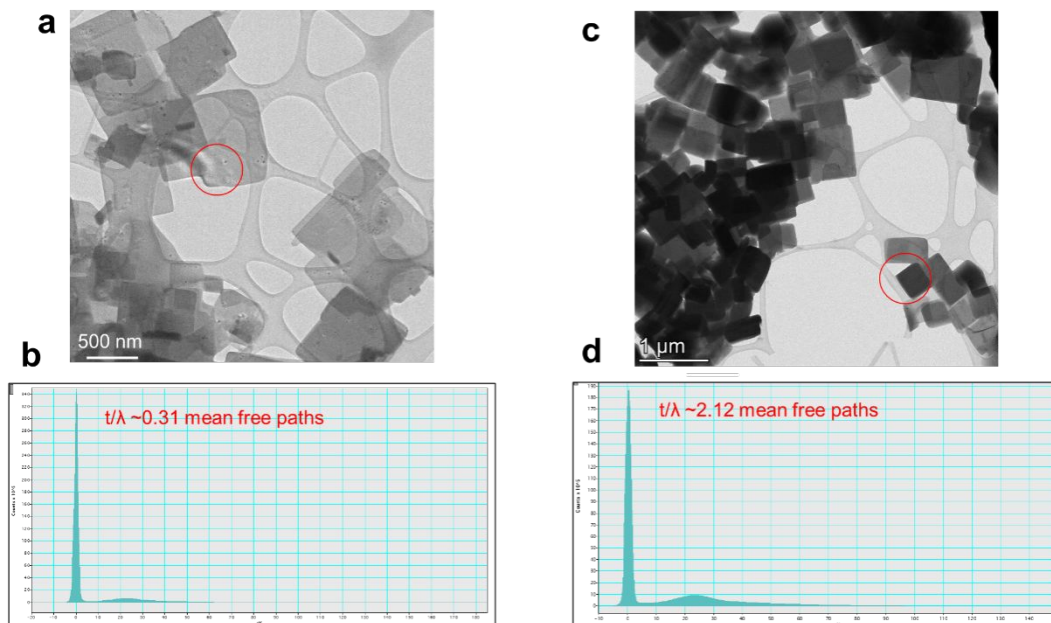

Fig. S2. The thickness of MAPbI$_3$ NPLs has been estimated from the plasma peak and zero-peak ratio in EELS at 60 kV. Thus, the t/λ values can be calculated based on Log-Ratio method[1] by a plug-in tool in the DigitalMicrograph software, shown in the figures S2c-d. The mean free path of MAPbI$_3$ was assumed to be 48 nm according to references.[1-2] Therefore, for the NPLs shown in (a) their thickness is 15 nm (1 h aged sample) and the corresponding EELS shown in (b). For the NPL shown in (c), it is 102 nm for 9 h aged sample, related to the EELS in (d).

References

1. Malis et al., J. Electron Microsc. Tech. vol. 8 (1988) p193.
2. Iakoubovskii et al., Microscopy Research and Technique, vol. 71 (2008) p626.

2.3 Simulated diffraction pattern of the MAPbI₃ structure

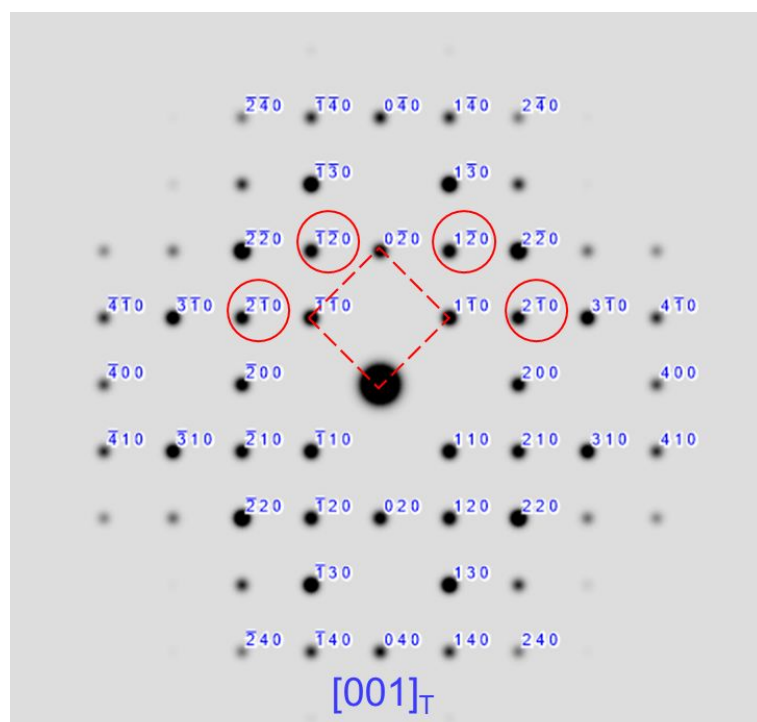Fig. S3 Simulated electron diffraction pattern of the tetragonal MAPbI$_3$ perovskite structure (S.G. *I422*) along [001]$_T$ direction, performed using the CrystalDiffraction software. The red dashed rectangle represents the diffraction pattern corresponding to the pseudo-cubic perovskite structure. The characteristic diffraction spots of the tetragonal MAPbI$_3$ perovskite structure are marked by red circles.

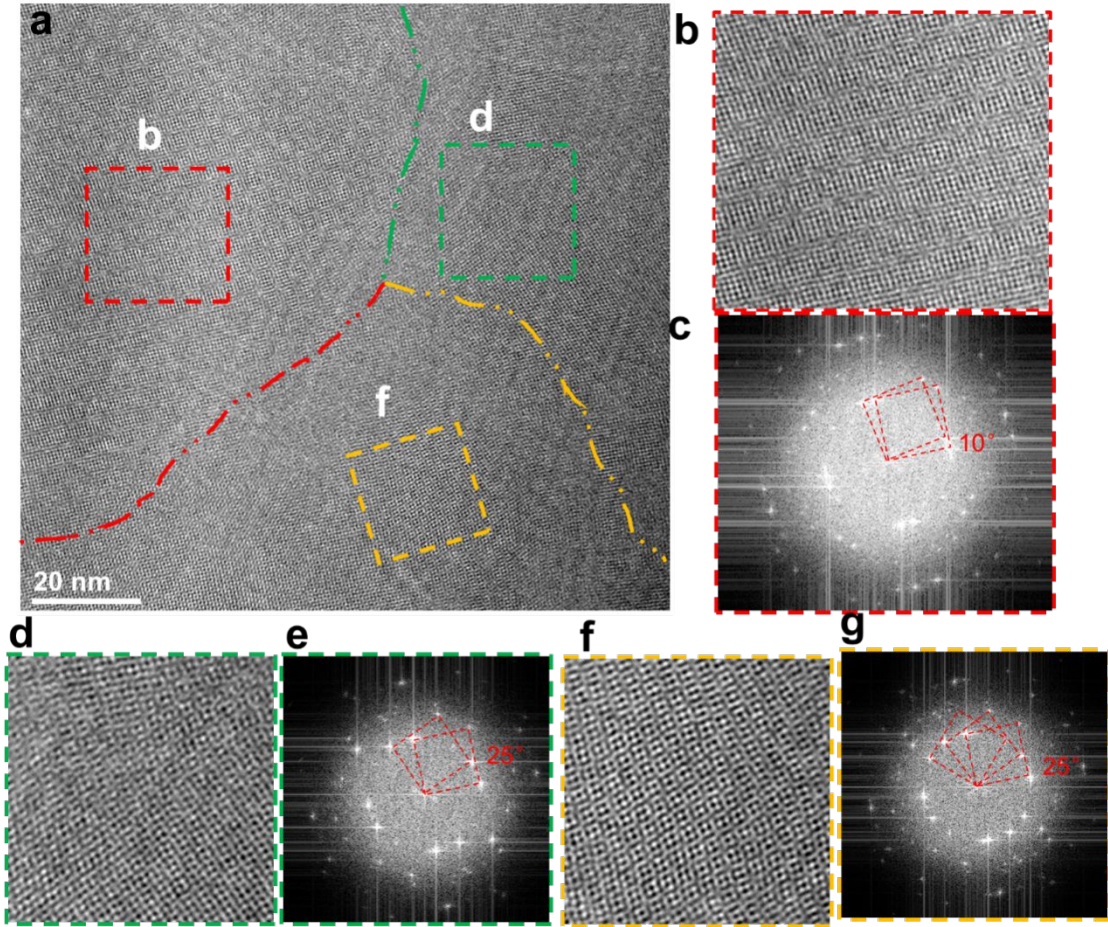## 2.4 High resolution cryo-TEM images of MAPbI$_3$ NPLs in the fresh sample

Fig. S4 (a) HRTEM image of the 0 h MAPbI$_3$ NPL displaying 3 different types of rotational morié patterns, which are emphasized by red, yellow and green boundaries. (b) 10-degree morié patterns enlarged from the red box in (a), and its corresponding FFT pattern (c), which show the same type of rotational morié fringes as shown in Figure 2 in the main text. Frames (d) and (e) show the HRTEM image and the corresponding FFT pattern of the two monolayers with 25-degree rotational morié fringes, respectively. Frames (f) and (g) show the HRTEM image and the correspondent FFT pattern of three monolayers overlapped with 25-degree rotational morié fringes, respectively.

Apart from the 10-degree rotation moiré fringes, there are several kinds of twisted perovskite monolayers with different rotation angles which can be observed in the 0 h MAPbI$_3$ NPLs. Based on the observed rotational moiré fringes, monolayers with twist boundaries of 10, 25 and 50 rotation angles are displayed in Figure S3, demonstrating that the formation of the twisted monolayers is a common phenomenon at the initial stages of formation of MAPbI$_3$ perovskite NPLs.

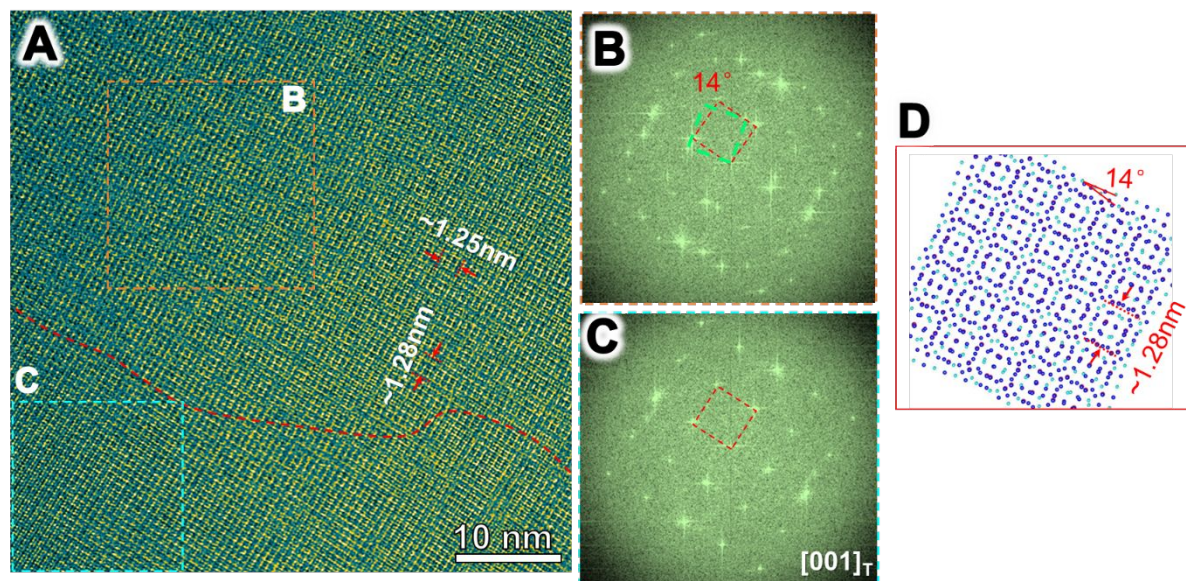## 2.5 The interface of twisted lattices and single-crystalline MAPbI$_3$ nanoplatelet

Figure S5. (a) Cryo-HRTEM image demonstrating the interface between two rotated monolayers with twisted lattices (top) and single-crystalline MAPbI$_3$ nanoplatelet (bottom) in the 0 h NPL sample. The accumulated electron dose for this HRTEM image is about 5.98 e/A^2. (b) FFT pattern of the twisted lattice area (dashed brown square) above the dotted red line in (a). (c) FFT pattern of the single-crystalline area from dashed cyan square in (a). (d) A model of the twisted lattice with two 14° rotation monolayers, being consistent with HRTEM image area above the red line in (a).

Figure S5 demonstrates the boundary area between MAPbI3 rotated monolayers (top) and a single NPL (bottom) in the fresh sample. At the bottom, it is an ideal single-crystalline MAPbI$_3$ atomic structure along [001]$_T$ direction, which we will analyze in details below. The rotational moiré fringe features a repeating unit distance of ~1.25 nm. The corresponding FFT pattern obtained from the rotational moiré fringes illustrates that the overlapping monolayers are twisted 14 degrees from each other, as shown by their diffraction patterns marked by red and green squares in Figure S4b. We notice that in Figure S4b the contrast of the red sets of diffraction patterns is stronger than that of the green ones, which means that fewer accountings of the 14-degree rotated monolayer exist on the bottom MAPbI$_3$ NPL. FFT pattern of dashed cyan square in (a) demonstrated one set of [001]$_T$ diffraction pattern from a single-crystalline MAPbI$_3$ layer. Figure S4d provides the structure model of the rotational moiré fringes observed here.
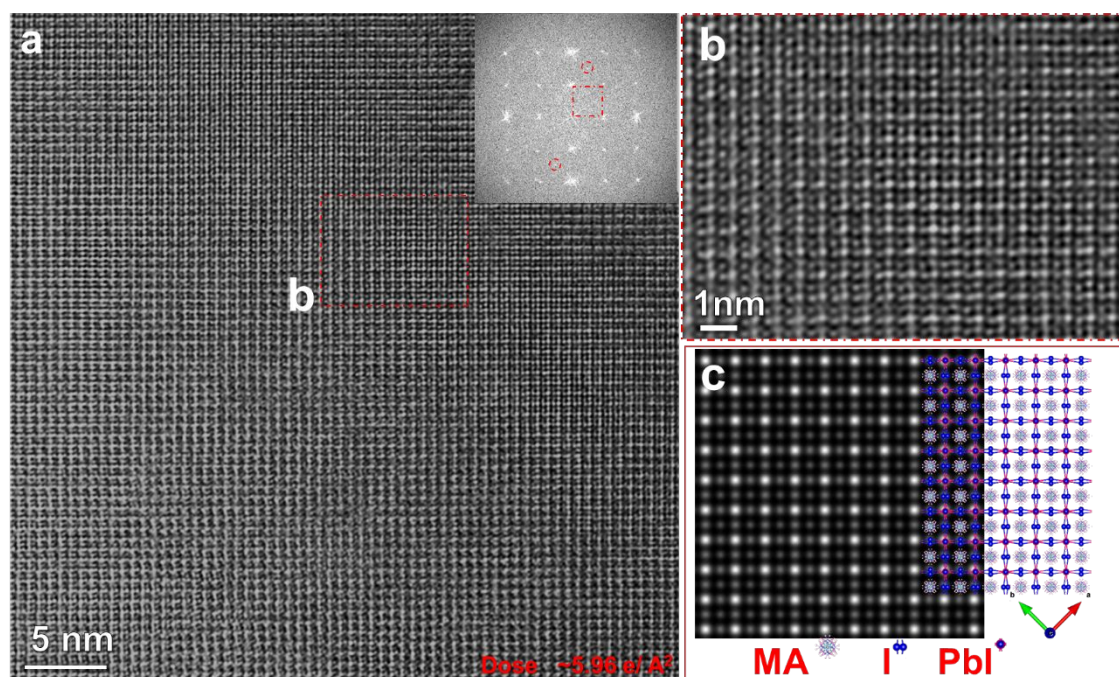
2.6 Grayscale image of Figure 5

Fig. S6 Grayscale HRTEM image of Figure 3.

2.7 HRTEM image simulation results of the MAPbI$_3$
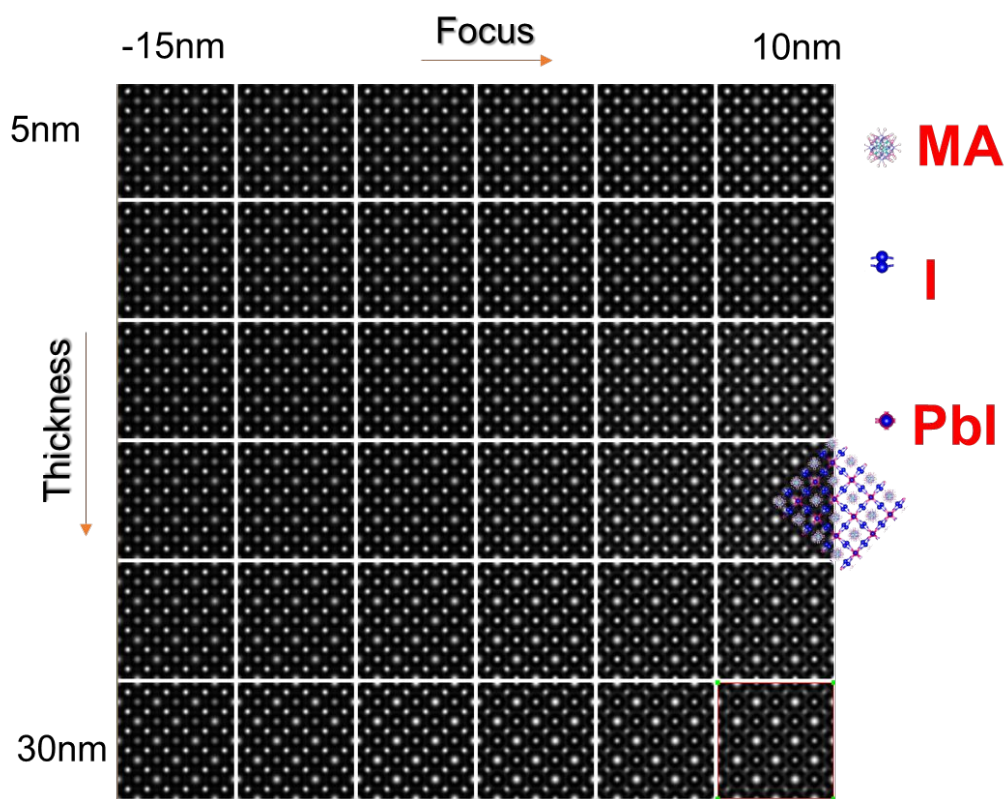

Fig. S7 Simulation results for the HRTEM image of the MAPbI$_3$ structure along the [110]$_T$ direction performed by MacTempas using the multi-slice simulation. The image at the middle right side is the corresponding tetragonal structure model along [110]$_T$ direction showing positions of the atomic columns. The thickness ranges from 5 nm to 30 nm, while the defocus ranges from -15 nm to 10 nm. The simulated image used in the manuscript is at the defocus value of 5 nm, and the thickness value of 15 nm.

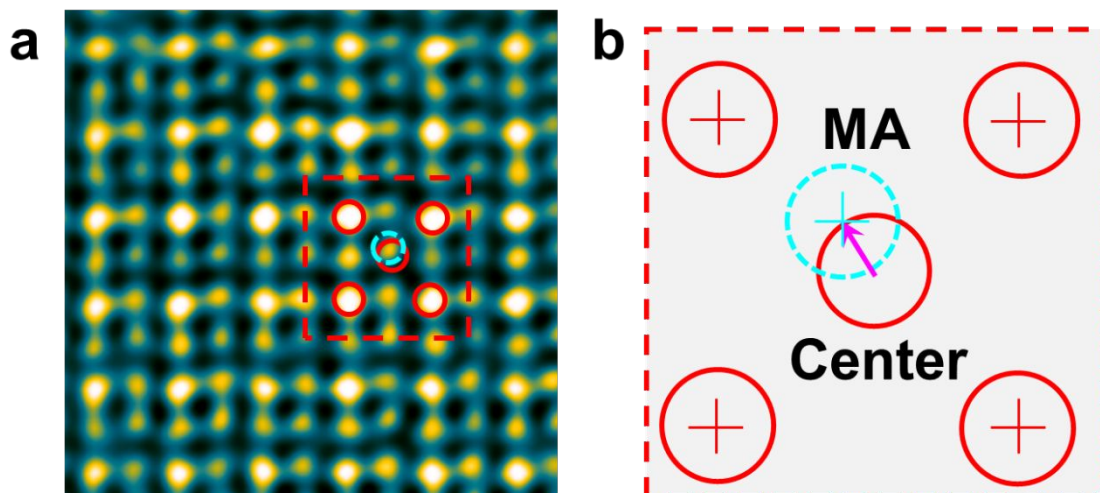## 2.8 Quantitate analysis of the polarization of MA ions.

Fig. S8 Quantitate analysis of the MA ions polarizations. (a) Cryo-HRTEM image of the [001] MAPbI$_3$ structure. (b) Schematics for the polarization of an MA ion used in the calculation. Atomic columns positions are determined by Gaussian fitting performed in the MacTempas X software. The MA polarization can be defined to be the deviation between the real MA position (cyan dashed circle) and the ideal position (red center circle) surrounded by 4 PbI columns (red circles with "+"). This step was performed in the Matlab software.

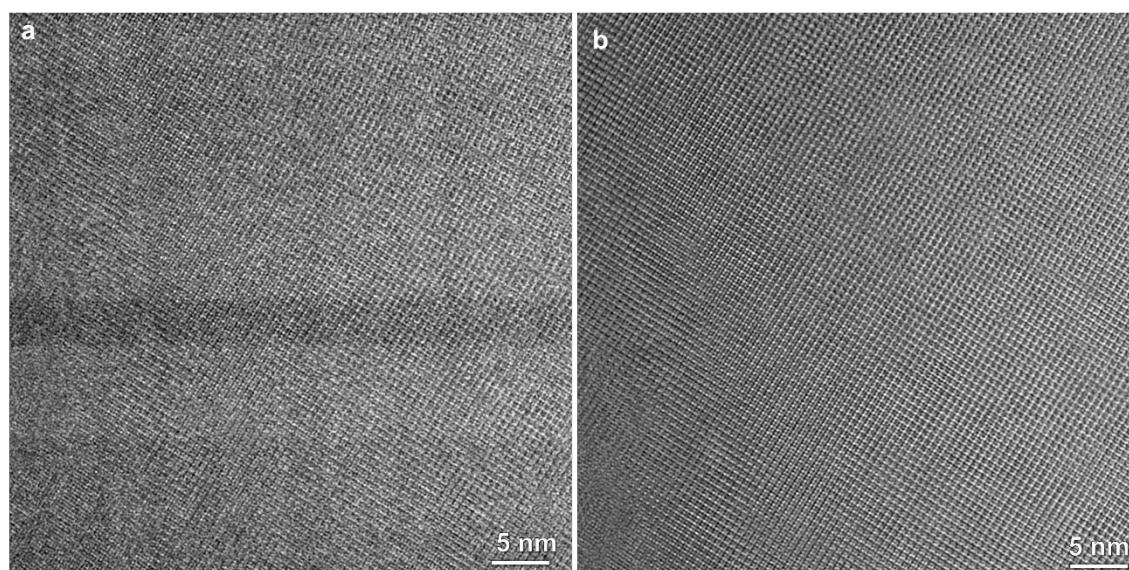## 2.9 Comparison of the raw and filtered HRTEM images

Fig. S9 A Comparison of the HRTEM image for (a) raw (unfiltered), and (b) Bragg-filtered data for 1h MAPbI$_3$ NPLs.

2.10 calculated structure models and details

A slab structure of the (001) surface with 4 unit layers is used to model the perfect MAPdI$_3$ surface. Two twisted bilayers with a twisted angle using accidental angular commensurations (Figure S10) are used to simulate the twisted MAPdI$_3$. To avoid strain effect between two bilayers, the basis vectors of two bilayers are selected as the integral summation of two basis vectors of the MAPdI$_3$ unit cell (denoted as a1 and a2). As presented in Figure S10, a twisted bilayer with a basis vector $n_{a1}+m_{a2}$ stacks on a commensurate bilayer with a corresponding basis vector ($n_{a1}-m_{a2}$). Such a twisted model has a corresponding twisted angle, $\theta = 2\tan^{-1}(m/n)$. Here, we simulated three different twisted models with angles at 53°, 37° and 22°, respectively. The number of total atoms in models are 240, 480, 816 and 1248, respectively. Further decreasing the twist angle to 14° enlarges the system a lot (containing 3120 atoms) that makes computational cost too expensive.
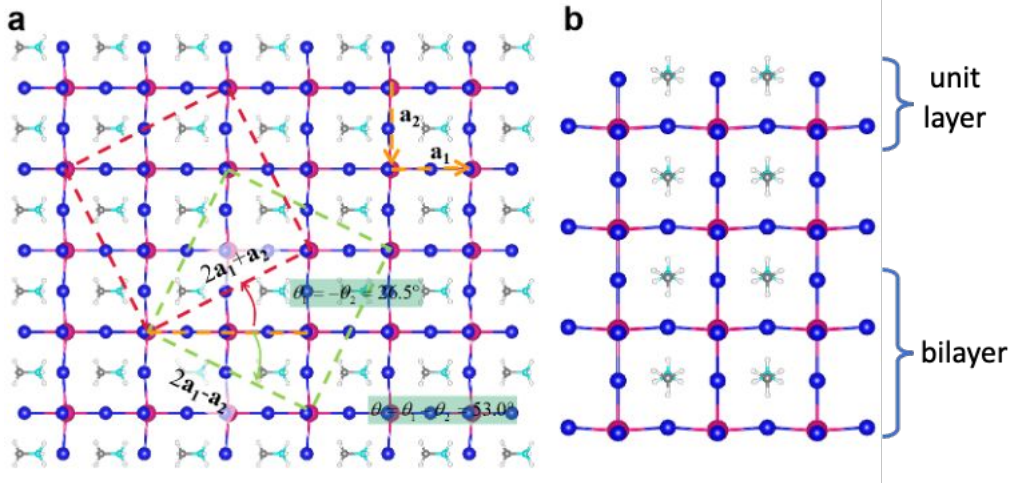

Figure S10. (a) Schematic illustration of the construction approach from the perfect structure to the twisted configuration. (b) Definition of a unit layer and bilayer in the MAPbI$_3$.
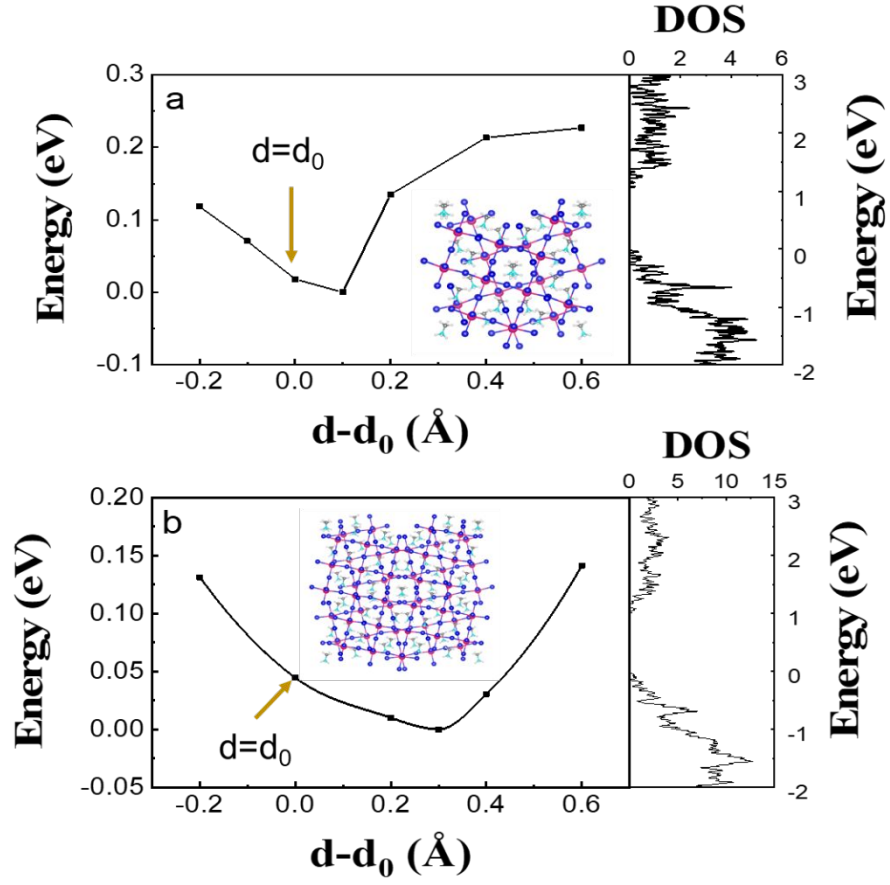
Figure S11. Energy variation (the left panel) with the distance difference between two bilayers and the density of states (the right panel) of the twisted MAPdI$_3$ layers with a twisted angle (a) 37° and (b) 22°. The most stable structure for each twisted model is shown in the inset images.